Biphoton topology in a quadratic nonlinear waveguide array under the Su-Schrieffer-Heeger model

Ying Yang,[1,2,*] Zhengwei Zuo,[3] and Dawei Cao[1]

[1]*School of Physics and Electronic Engineering, Jiangsu University, Zhenjiang 212013, People's Republic of China*

[2]*Key Laboratory of Semiconductor Materials Science, Beijing Key Laboratory of Low Dimensional Semiconductor Materials and Devices, Institute of Semiconductors, Chinese Academy of Sciences, Beijing 100083, China*

[3]*School of Physics and Engineering, Henan University of Science and Technology, Luoyang 471023, People's Republic of China*

(Received 18 November 2020; revised 5 October 2021; accepted 14 October 2021; published 28 October 2021)

We demonstrate the generation of a stable topologically nontrivial biphoton state with a high degree of quantum entanglement by the bosonic Bogoliubov Hamiltonian in a quadratic nonlinear waveguide array (QNWA) under the Su-Schrieffer-Heeger model. Analysis of its energy spectrum and eigenmode spectra verifies that this biphoton state is a topological nontrivial edge state characterized by the nonzero Berry phase at $1/4$ and $3/4$ fillings. The changes of Berry phase at $1/4$ and $3/4$ fillings indicate the topological quantum transition. The topological robustness of the biphoton edge state can be demonstrated by the spatial correlation under random disorders in propagation constant of the QNWA. It is also shown that the Rényi entanglement entropy of this topologically nontrivial biphoton state can approach high values. The robustness of this topologically nontrivial property suggests the promising application of this highly entangled biphoton state in quantum computing and information.

DOI: 10.1103/PhysRevA.104.043710

I. INTRODUCTION

Topological photonics has attracted a considerable amount of attention since Haldane and Raghu first applied topology to photonics in 2008 [1,2]. In the succeeding years, a series of theoretical and experimental studies have been carried out [3]. The wave property of light enables itself a perfect candidate for mimicking topological effects such as quantum Hall effect [4], time-reversal invariant topological insulators [5], and Floquet topological insulators [6,7]. At the same time, the application of topological features allows for the novel fabrication of integrated photonic devices, such as reflection-free waveguides, robust delay lines, spin-polarized switches, and nonreciprocal devices [8]. Topological methods have been used in photonics applications involving a variety of materials [9–12], dimensionalities [13–15], and regions of electromagnetic spectrum [5,16,17]. As a simple model, the Su-Schrieffer-Heeger (SSH) model has been extensively studied in both condensed matter physics and topological photonics, and various aspects of SSH models have been used to explore new phenomena [17]. Recently, SSH models have attracted a significant amount of attention as tools for understanding the structures of numerous topological phenomena and for facilitating both research and manufacturing [18–22]. however, further research is needed, particularly in the field of quantum topological photonics [23].

Optically nonlinear topologies were reported during the research of solitons [24–26] under a topological band. The resulting research has focused considerable theoretical and experimental interest in the topological phenomena of interacting photons [27–31], including a parametric process generated by the second-order nonlinear susceptibility $\chi^{(2)}$, in which the photon number is no longer conserved and the bosonic Bogoliubov Hamiltonian is gapless at zero energy but has nonzero gaps with topological edge state [32]. The susceptibility $\chi^{(2)}$ is the key parameter of spontaneous parametric down-conversion (SPDC) in the generation of biphotons in quantum optics. Quadratic nonlinear waveguide arrays (QNWAs) have shown a unique advantage in the manipulation of biphoton states [33–38] arising from the fact that the combination of SPDC and evanescent coupling produces additional quantum interference in these states [39]. The distribution of the biphoton in QNWAs also enables an entirely different quantum walk [40]. Recently, QNWAs have been utilized to mimic lattice topologies [41] and to produce Anderson localization [42], suggesting the possibility of applications in topological photonics and quantum simulation. The inherently wave-particle duality of biphotons endows itself a greater superiority than the classical light with only wave property as simulators in topological photonics [23,43–45], and biphotons have also drawn great attention in terms of their robustness as quantum topological edge states in quantum information and computation.

In this paper, a stable topologically nontrivial biphoton state with high quantum entanglement is demonstrated theoretically in a quadratic nonlinear waveguide array (QNWA) under the SSH model. We show that, if all of the waveguide channels are excited by pump light as an initial condition, the eigenvalues of the energy spectrum will all be real, thereby avoiding the parametric instabilities caused by the possible presence of complex eigenvalues in the bosonic Bogoliubov Hamiltonians. By analyzing the energy spectrum and eigenmode spectra, the topological nontrivial biphoton state and its

*yingyang@ujs.edu.cn

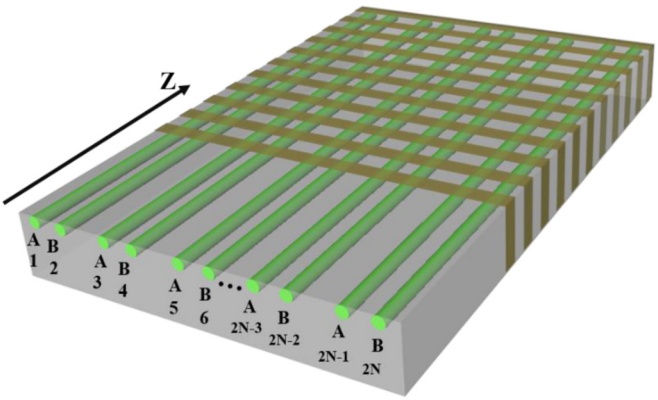

FIG. 1. Sketch of the QNWA under the SSH model is given. The green areas show waveguide channels dimerized under SSH model; the brown indicates domain reversal region of the SPDC process. Both pump light and biphotons propagate along the Z axis.

topological transition can be verified. It is also demonstrated that, as a result of its spatial correlation, the topological nontrivial biphoton state is intensively located in the first and last waveguide channels of the QNWA and, therefore, that the biphoton eigenmode indicates a biphoton edge state. This biphoton edge mode is shown to be preserved under the random disorder of propagation constant β_0, which also strongly suggests a topologically protected biphoton state.

II. MODEL

Figure 1 gives a sketch of the QNWA under the SSH model. The array is designed by applying a binary coupling strength between waveguide channels, based on the binary distance between adjacent waveguide channels as show in Fig. 1. A binary coupling, namely two different coupling strengths, is designed to achieve a dimerized SSH model. In this array, there are two different distances (a binary distance) between adjacent waveguide channels, so that the biphoton can hop to the left channel and right channel with two different coupling strengths. The QNWA material can be lithium niobate (LN) and fabricated into waveguides by using either a proton-exchange or titanium-diffusion method. By this model, the SPDC process can be achieved in, for example, periodically poled lithium niobate (PPLN). We take the PPLN as a method to achieve the SPDC process in QNWA and the perfect phase matching is significant in the SPDC process. As discussed by other researchers [33,41], there are two kinds of the phase mismatch, namely, the spectral phase mismatch in a single waveguide channel and the space phase mismatch induced by the dispersion of the QNWA. In the following discussion, the type-0 degenerate SPDC process is considered, which means the signal and idler photons share the same frequency and polarization and therefore that the spectral phase mismatch satisfying the zero-order phase mismatch can be set to zero theoretically. Once the dispersion of the QNWA is identified, the possible momentum correlations of the biphoton are given by the space phase mismatch, and the final momentum correlations of the biphoton are determined by which correlation is selected by the initial distribution of pump light, as discussed in [34,38]. The domain reversal region covers all $2N$ waveguide channels. Under the SSH model, the biphoton Hamiltonian in the QNWA can be described by using the Schrödinger formulation as follows:

$$\begin{aligned} H &= H_{\mathrm{SSH}} + H_{\mathrm{SPDC}}, \\ H_{\mathrm{SSH}} &= \sum_{q,\alpha=s,i}^{2N} \beta_0 \hat{C}^{\dagger}_{q,\alpha}\hat{C}_{q,\alpha} + (\kappa_0 + (-1)^q \delta\kappa)\hat{C}^{\dagger}_{q+1,\alpha}\hat{C}_{q,\alpha} \\ &\quad + \mathrm{H.c.}, \\ H_{\mathrm{SPDC}} &= \sum_{q}^{2N} \chi^{(2)}\hat{C}^{\dagger}_{q,s(i)}\hat{C}^{\dagger}_{q,i(s)} + \mathrm{H.c.}, \end{aligned} \tag{1}$$

where H_{SSH} and H_{SPDC} are the SSH model and SPDC Hamiltonians, respectively. β_0 is the propagation constant of each waveguide channel, and $\hat{C}^{\dagger}_{q,\alpha}$ ($\hat{C}_{q,\alpha}$) is the creation and annihilation operators, respectively, for the signal ($\alpha = s$) and idler ($\alpha = i$) photons in the q^{th} waveguide channel. $\chi^{(2)} = id_{\mathrm{eff}}$ is the second order nonlinear susceptibility and d_{eff} is the effective nonlinear coefficient. In addition, $\kappa_0 + (-1)^q\,\delta\kappa$, the binary coupling strength in a one-dimensional (1D) dimerized SSH model [46], can be easily achieved experimentally by binary distant shift between adjacent waveguide channels [47]. The waveguide channels are assumed to be single mode for biphoton, as well as the binary coupling strength, so the pump light will not couple in this array and only the biphoton can hop between channels since the wavelength of the biphoton is twice that of the pump light in the type-0 degenerate SPDC process.

From $i\frac{d\hat{A}^{\dagger}}{dt} = [\hat{A}^{\dagger}, H]$, the Heisenberg equation of the creation operator of the signal (idler) photon in the q^{th} waveguide channel can be given as

$$\begin{aligned} i\frac{\partial \hat{C}^{\dagger}_{q,\,s(i)}}{\partial z} &= \beta_0\hat{C}^{\dagger}_{q,s(i)} + [\kappa_0 - (-1)^q\delta\kappa]\hat{C}^{\dagger}_{q+1,s(i)} \\ &\quad + [\kappa_0 + (-1)^q\delta\kappa]\hat{C}^{\dagger}_{q-1,s(i)} + \sum_{q}^{2N}\chi^{(2)*}\hat{C}_{q,i(s)}. \end{aligned} \tag{2}$$

The entire biphoton Hamiltonian, including the SPDC, can then be transformed into a wave-vector-dependent one for both signal and idler photons. To simplify this transformation, the biphoton Hamiltonian can be rewritten as

$$\begin{aligned} H_{\mathrm{SSH}} &= \sum_{r,\alpha=s,i}^{N} [\beta_0(\hat{A}^{\dagger}_{r,\alpha}\hat{A}_{r,\alpha} + \hat{B}^{\dagger}_{r,\alpha}\hat{B}_{r,\alpha}) + \kappa_{-}\hat{A}^{\dagger}_{r,\alpha}\hat{B}_{r,\alpha} \\ &\quad + \kappa_{+}\hat{A}^{\dagger}_{r+1,\alpha}\hat{B}_{r,\alpha}] + \mathrm{H.c.}, \\ H_{\mathrm{SPDC}} &= \sum_{r}^{N}\chi^{(2)}\hat{A}^{\dagger}_{r,s(i)}\hat{A}^{\dagger}_{r,i(s)} + \hat{B}^{\dagger}_{r,s(i)}\hat{B}^{\dagger}_{r,i(s)} + \mathrm{H.c.}, \end{aligned} \tag{3}$$

where $\hat{A}^{\dagger}_{r,\alpha}(\hat{B}_{r,\alpha})$ is the creation and annihilation operators for biphotons on $A(B)$ subwaveguide array (sub-WA) standing for the odd and even numbered waveguide sets as labeled in Fig. 1. $\kappa_{-} = \kappa_0 - \delta\kappa$ and $\kappa_{+} = \kappa_0 + \delta\kappa$ are the binary coupling strengths. $\delta\kappa$ is the dimerized coupling strength. In this QNWA model, each waveguide channel q^{th} can be considered as a source of biphotons if the pump light is excited in this

channel. We assume all channels are excited, which means the SPDC process (the generation of biphotons) occurs in every channel of the QNWA along the propagation direction. This assumption can be achieved by the summation of all channels in the array of H_{SPDC} in both Eqs. (1) and (3), namely there are $2N$ terms in H_{SPDC}. By performing the Fourier transformations $\hat{a}^{+}_{k_\alpha} = \frac{1}{\sqrt{N}} \sum_r e^{ik_\alpha \cdot rd} \hat{A}^{+}_{\alpha,r}$ and $\hat{b}^{+}_{k_\alpha} = \frac{1}{\sqrt{N}} \sum_r e^{ik_\alpha \cdot rd} \hat{B}^{+}_{\alpha,r}$, where d is the waveguide structure period in the QNWA transverse direction and k_α is the transverse wave vector of the signal and idler photons, the bosonic Bogoliubov Hamiltonian can be obtained in reciprocal space. During this transformation, all waveguide channels are assumed to be excited with pump light, i.e., the SPDC process occurs in every channel of the QNWA along the propagation direction. This initial condition requires that, for the transverse wave vectors of the signal and idler photons, $\delta(k_s + k_i) = 0$, that is, that $k_s = -k_{\mathrm{i}}$ when $r \to \infty$. Assuming that $k_s = -k_i = k$, the bosonic Bogoliubov Hamiltonian in reciprocal space can be described by introducing the operator $\hat{C}^{\dagger}_k = (\hat{a}^{\dagger}_k, \hat{b}^{\dagger}_k, \hat{a}_{-k}, \hat{b}_{-k})$,

$$H = \frac{1}{2} \sum_k \hat{C}^{\dagger}_k H(k) \hat{C}_k$$

with

$$H(k) = \begin{pmatrix} \beta_0 & \kappa^* & \chi^* & 0 \\ \kappa & \beta_0 & 0 & \chi^* \\ \chi & 0 & \beta_0 & \kappa^* \\ 0 & \chi & \kappa & \beta_0 \end{pmatrix}, \tag{4}$$

where $\kappa = \kappa_- + \kappa_+ e^{-ikd}$.

III. SPECTRUM ANALYSIS

The energy spectra ε of biphotons under the open boundary condition (OBC) and period boundary condition (PBC) with a fixed nonlinear coefficient $d_{\mathrm{eff}} = 1.5$ are shown in Figs. 2(a) and 2(b), respectively. The parameters $\kappa_0 = 1$, $\delta\kappa = [-1\text{–}1]$, $\beta_0 = 0$, and $2N = 64$ were used in carrying out these simulations (all energy parameters are scaled by κ_0, thus, dimensionless). A comparison between OBC and PBC spectra reveals that, when the dimerized coupling strength $\delta\kappa > 0$, in-gap edge modes are present, a hallmark of the nontrivial topological properties of the system. Because $k_s = -k_i$ under the assumed initial conditions, it is not difficult to show that all of the eigenvalues in the energy spectrum are real, allowing for the use of the bosonic Bogoliubov Hamiltonian in Eq. (3) and obeying the particle-hole symmetry and more stable topological edge states shown in Fig. 2(c). As demonstrated in Fig. 2(d), the biphoton eigenmodes tend to locate at the two ends of the array ($\delta\kappa = 0.7$), a typical topological edge state behavior under OBC. To further determine the topological properties of these two biphoton states, the Berry phases of the biphoton edge states can be calculated [48]. For 1/4 and 3/4 filling cases, the Berry phases are both equal to 0.5 (in the unit of 2π) as shown in Figs. 3(a) and 3(b), respectively, verifying the presence of the nontrivial biphoton states. The topological phase transition occurs at $\delta\kappa = 0$. It is clear that the introduction of $\chi^{(2)}$ to the Hamiltonian provides an "interaction" between the signal and idler photons; therefore, their propagation in the WA cannot be considered to reflect the independent particle hopping behavior of pairs of single particles but rather must be accounted for as interactional particle hopping behavior in the SSH lattice.

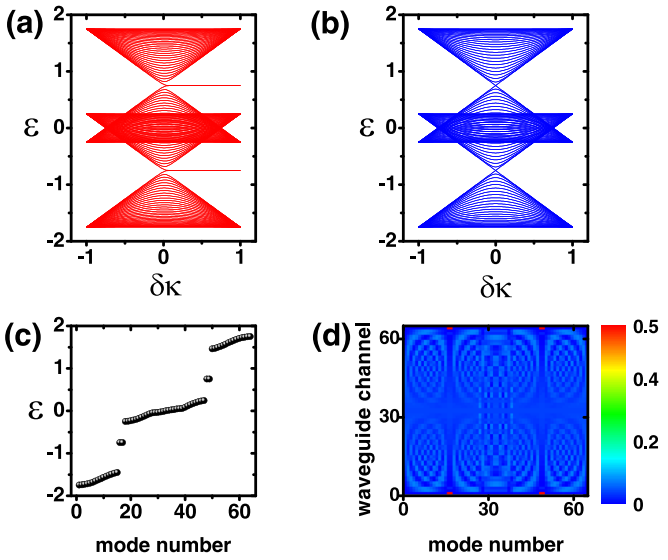

FIG. 2. Biphoton energy spectra ε under (a) OBC and (b) PBC ($d_{\mathrm{eff}} = 1.5$, $\kappa_0 = 1$, $\delta\kappa = [-1\text{–}1]$, $\beta_0 = 0$ and $2N = 64$). (c) Eigenmode spectra ε of biphoton at $\delta\kappa = 0.7$ under OBC. (d) Distribution of biphoton eigenmodes with the same simulation parameters in (c) .

IV. SPATIAL CORRELATION

We next consider the spatial correlation of the biphoton states under the OBC. The bosonic creation operators in the n^{th} waveguide channel at position z along the propagation direction can be described as

$$\hat{a}^{\dagger}_n(z) = \sum_m U_{nm}(z) \hat{a}^{\dagger}_m(0), \tag{5}$$

where $U_{nm}(z) = e^{-iHz}$ is a unitary transformation matrix in real space induced by the time-dependent evolution of the Hamiltonian in Eq. (1) [49], which provides the amplitude of the biphoton state in the n^{th} waveguide channel when the m^{th} waveguide channel is excited by the pump light. Since

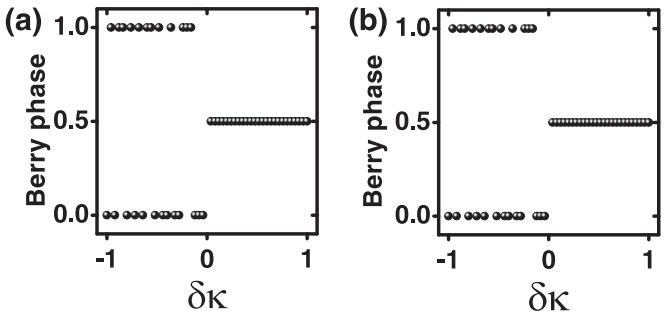

FIG. 3. The Berry phase (in units of 2π) of the biphoton states for (a) 1/4 filling and (b) 3/4 filling cases corresponding to $\delta\kappa$ varying from -1 to 1 with other simulation parameters set as $d_{\mathrm{eff}} = 1.5$, $\kappa_0 = 1$, and $\beta_0 = 0$.

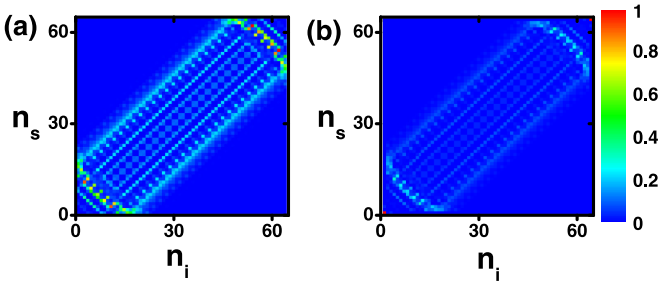

FIG. 4. Spatial correlation of biphotons in real space (n_s and n_i are the waveguide channels for signal and idler photon, respectively) in (a) topologically trivial ($\delta\kappa = -0.7$) and (b) nontrivial biphoton states ($\delta\kappa = 0.7$) with $d_{\text{eff}} = 1.5$, $\kappa_0 = 1$, $\beta_0 = 0$, $z(\text{a.}u.) = 10$, and $2N = 64$.

all of the channels are excited, the total number of excited channels is $2N$. The spatial correlation, namely, the second-order correlation function in real space, is

$$\Gamma_{si} = \langle \hat{a}_s^\dagger \hat{a}_i^\dagger \hat{a}_i \hat{a}_s \rangle = |\langle 0|\hat{a}_i \hat{a}_s \hat{a}_m^\dagger \hat{a}_n^\dagger|0\rangle|^2 = \sum_m |U_{sm}U_{im} + U_{im}U_{sm}|^2. \quad (6)$$

In the QNWA, the photon pairs generated at different positions along the direction of propagation in identical waveguide channels exhibit coherence, which makes it theoretically and experimentally possible to achieve various biphoton quantum states [36,50–52]. Because the photon pairs produced in different waveguide channels are incoherent, it is possible to make an incoherent superposition of the individual second-order correlation functions produced by different pump light-excited waveguide channels as shown in Eq. (5). A numerical simulation of the spatial correlation of biphoton states with the parameter settings $d_{\text{eff}} = 1.5$, $\kappa_0 = 1$, $\beta_0 = 0$, $z(\text{a.u.}) = 10$, and $2N = 64$ is shown in Fig. 4. n_s and n_i are the waveguide channels for signal and idler photon, respectively. The figure shows (a) topologically trivial ($\delta\kappa = -0.7$) and (b) topologically nontrivial ($\delta\kappa = 0.7$) biphoton states. In the former [Fig. 4(a)], the signal and idler photons tend to scatter into the WA, even though the transverse wave vector of the biphotons in reciprocal space shows anticorrelation ($ks = -ki$) because each waveguide channel is excited by pump light in real space. As the biphoton state is transmitted from a topologically trivial state to a nontrivial state, both the signal and idler photons tend to remain in the 1st and 64th waveguide channels, verifying the presence of a topologically nontrivial biphoton edge state as shown in Fig. 2(d).

In general, the edge states are topologically protected against disorders to preserve chirality under the SSH model. To verify this, a random disorder can be introduced to the propagation constant β_0. The disorder we introduced is a random change of the propagation constant β_0, namely, β_0 is no longer a constant for every channel in array (each channel q^{th} has a fixed β_{q}). The ratio 50% (90%) refers to β_{q} varying from 0 to 0.5 (0 to 0.9) randomly, since all energy parameters are scaled by κ_0, thus, dimensionless. Figure 5 shows the spatial correlations of the topologically trivial [$\delta\kappa = -0.7$ in Figs. 5(a) and 5(b)] and nontrivial [$\delta\kappa = 0.7$ in Figs. 5(c) and 5(d)] biphoton states under 50% [Figs. 5(a)–5(c)] and

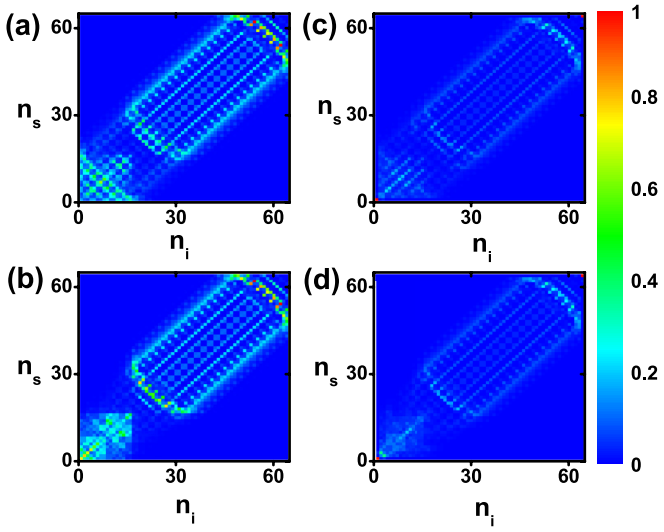

FIG. 5. Spatial correlation and probability amplitudes in real space (n_s and n_i are the waveguide channels for signal and idler photon, respectively) of trivial and nontrivial biphoton states in the presence of a random disorder in propagation constant. (a), (b) and (c), (d) show the spatial correlation of topologically trivial and nontrivial biphoton states under 50% and 90% disorder, respectively. Other simulation parameters are $d_{\text{eff}} = 1.5$, $\kappa_0 = 1$, $z(\text{a.u.}) = 10$ and $2N = 64$.

90% [Figs. 5(b)–5(d)] disorder, respectively. The other simulation parameters are $d_{\text{eff}} = 1.5$, $\kappa_0 = 1$, $z(\text{a.u.}) = 10$ and $2N = 64$. Figures 5(a) and 5(b) demonstrate the spatial correlation of trivial biphoton state under 50% and 90% disorder, respectively. These distributions of the spatial correlation are skewed with respect to those without disorder shown in Fig. 4(a), since the propagation constant β_{q} in each q^{th} channel is not homogeneous but biased. For a nontrivial biphoton state, Figs. 5(c) and 5(d) demonstrate the spatial correlation under 50% and 90% disorder, respectively. This time, both the signal and idler photons remain in the 1st and 64th waveguide channels under 50% and 90% disorder, implying the robustness against disorders to preserve chirality. By comparison, the signature of topological protection is prominent in nontrivial biphoton states with disorders.

In the proceeding discussion, we verified that the biphoton states generated in the QNWA of the SSH model are topologically nontrivial edge states. It is also worth determining if the quantum entanglement of these biphoton states is also associated with their topological properties. To assess this, we calculate the Rényi entanglement entropy [43,53]. The biphoton wave function in real space can be given as

$$|\varphi\rangle = \sum_n \alpha_{nn}|1_n 1_n\rangle + \sum_{m\neq n} \alpha_{mn}|1_m 1_n\rangle, \quad (7)$$

where $\alpha_{\text{nn}}(\alpha_{\text{mn}})$ are the probability amplitudes of the signal and idler photons located at the identical waveguide channel n^{th} and different m^{th} and n^{th} waveguide channels, respectively. The Rényi entanglement entropy can be defined as

$$\text{S} = -\log_2 \text{Tr}\rho_1^2, \quad (8)$$

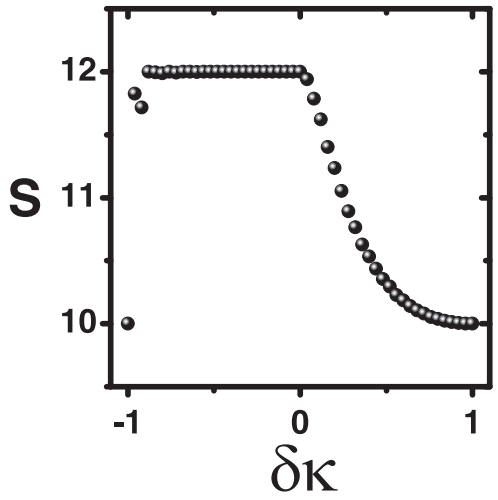

FIG. 6. Rényi entanglement entropies S corresponding to $\delta\kappa$ =[−1–1] with $d_{\text{eff}} = 1.5$, $\kappa_0 = 1$, z(a.u.) = 10, and $2N = 64$.

where $\rho_1 = \text{Tr}_2\rho$ is the reduced density matrix obtained by tracing out the second photon variables from the biphoton density matrix $\rho = |\varphi\rangle\langle\varphi|$. From this, we obtain

$$\text{Tr}\rho_1^2 = 4\sum_{n=1}^{2N}|\alpha_{nn}|^4 + 8\sum_{n=1}^{2N} f_n|\alpha_{nn}|^2 + 4\sum_{n=1}^{2N} f_n^2, \quad (9)$$

$$f_n = \sum_{m=1}^{n-1}|\alpha_{mn}|^2, \quad (10)$$

which are in accordance with Eqs. (23) and (24) in [43]. Figure 6 shows the results of a numerical simulation of the Rényi entanglement entropy corresponding to $\delta\kappa = [-1\text{–}1]$ with $d_{\text{eff}} = 1.5$, $\kappa_0 = 1$, z(a.u.) = 10, and $2N = 64$. In the trivial zone ($\delta\kappa < 0$), the entanglement entropy changes to an insignificant degree and stabilizes at 12, after which ($\delta\kappa > 0$) it declines to 10. The Rényi entanglement entropy of biphoton states in real space shows a clear change around the topological transition point. The value of the Rényi entanglement entropy is primarily determined by the probabilities of the biphoton states, e.g., $|\alpha_{nn}|^2$ and $|\alpha_{mn}|^2$, which can be obtained experimentally by carrying out spatial coincidence counts in the QNWA during the spatial correlation measurement [52]. This makes it possible to read topological transitions directly through the experimental measurement of spatial correlation in real space. We also note that the effect of topological transition on the Rényi entanglement of the biphoton states is not extraordinary, as the rate of change of entanglement entropy during the topological transition is only 16.7%. As a result, the biphoton states, generated in the QNWA of the SSH model, are not only topologically nontrivial but also highly entangled, making them potentially useful in quantum computing and information applications.

V. CONCLUSION

In this paper, a stable topological nontrivial biphoton state with a high degree of quantum entanglement is demonstrated by bosonic Bogoliubov Hamiltonian in the QNWA under the SSH model. The choice of an initial condition, in which all waveguide channels are excited by pump light, makes it possible to avoid those parametric instabilities that can be caused by complex eigenvalues in the bosonic Bogoliubov Hamiltonian. Analysis of the energy spectrum, eigenmode spectra, and biphoton state distributions revealed that the topological transition point is identical to that under the general SSH model at $\delta\kappa = 0$. The Berry phases for the 1/4 and 3/4 filling cases are both equal to 0.5, conforming the presence of the topologically nontrivial biphoton states and, therefore, the establishment of a stable topologically nontrivial biphoton state. A comparison of the spatial correlations in the trivial and nontrivial zones under 50% and 90% random disorders confirmed the robustness of the biphoton edge mode. Using the Rényi entanglement entropy, it was shown that, although the influence of topological transition on the entanglement of the biphoton states is not significant, the states can be both highly entangled and topologically nontrivial. The robustness of topologically nontrivial property makes biphoton states more stable and protects them from decoherence during transmission [23,44]. Besides, some quantum photonic devices that are topologically protected, including topological beam splitters [54], quantum amplifiers [55], and quantum walks [56], have been realized recently. Comparing to those above applications, the topological biphoton states generated by our protocol can be highly entangled, which demonstrates itself as a promising candidate for applications in quantum computing and information.

ACKNOWLEDGMENTS

This work was supported by the Talent Fund of Jiangsu University (Grant No. 17JDG014), the project of Zhenjiang Key Laboratory of Advanced Sensing Materials and Devices (Grant No. SS2018001), the Innovation/Entrepreneurship Program of Jiangsu Province, and the project of Zhenjiang Key Laboratory of Advanced Sensing Materials and Devices (Grant No. SS2018001). Z.W.Z. is sponsored by Natural Science Foundation of Henan (Grant No. 212300410040). D.C. appreciates the support from the Jiangsu Specially-Appointed Professor Program.

[1] S. Raghu and F. D. M. Haldane, Phys. Rev. A **78**, 033834 (2008).

[2] F. D. M. Haldane and S. Raghu, Phys. Rev. Lett. **100**, 013904 (2008).

[3] T. Ozawa, H. M. Price, A. Amo, N. Goldman, M. Hafezi, L. Lu, M. C. Rechtsman, D. Schuster, J. Simon, O. Zilberberg, and I. Carusotto, Rev. Mod. Phys. **91**, 015006(76) (2019).

[4] Z. Wang, Y. Chong, J. D. Joannopoulos, and M. Soljačić, Nature (London) **461**, 772 (2009).

[5] X. Cheng, C. Jouvaud, X. Ni, S. H. Mousavi, A. Z. Genack, and A. B. Khanikaev, Nat. Mater. **15**, 542 (2016).

[6] F. Gao, Z. Gao, X. Shi, Z. Yang, X. Lin, H. Xu, J. D. Joannopoulos, M. Soljačić, H. Chen, L. Lu, Y. Chong, and B. Zhang, Nat. Commun. **7**, 11619 (2016).

[7] S. Mukherjee, A. Spracklen, M. Valiente, E. Andersson, P. Öhberg, N. Goldman, and R. R. Thomson, Nat. Commun. **8**, 13918 (2017).

[8] A. B. Khanikaev and G. Shvets, Nat. Photonics **11**, 763 (2017).

[9] S. Mittal, S. Ganeshan, J. Fan, A. Vaezi, and M. Hafezi, Nat. Photonics **10**, 180 (2016).

[10] K. Lai, T. Ma, X. Bo, S. Anlage, and G. Shvets, Sci. Rep. **6**, 28453 (2016).

[11] A. B. Khanikaev, S. H. Mousavi, W. Tse, M. Kargarian, A. H. Macdonald, and G. Shvets, Nat. Mater. **12**, 233 (2013).

[12] M. Di Liberto, A. Hemmerich, and C. MoraisSmith, Phys. Rev. Lett **117**, 163001 (2016).

[13] S. A. Skirlo, L. Lu, Y. Igarashi, Q. Yan, J. Joannopoulos, and M. Soljacic, Phys. Rev. Lett **115**, 253901 (2015).

[14] F. Li, H. Wang, Z. Xiong, Q. Lou, Y. Poo, J. Jiang, S. John, P. Chen, and R. Wu, Nat. Commun. **9**, 2462 (2018).

[15] S. Nolte, M. Segev, M. C. Rechtsman, J. M. Zeuner, A. Tu, and A. Szameit, Nat. Photonics **7**, 153 (2013).

[16] Y. Sun, D. Leykam, S. Nenni, D. Song, H. Chen, Y. D. Chong, and Z. Chen, Phys. Rev. Lett. **121**, 033904 (2018).

[17] S. H. Han, S. G. Jeong, S. W. Kim, T. H. Kim, and S. Cheon, Phys. Rev. B **102**, 235411 (2020).

[18] M. Yan, X. Huang, L. Luo, J. Lu, W. Deng, and Z. Liu, Phys. Rev. B **102**, 180102(R) (2020).

[19] Y. Gerasimenko, B. Tarasinski, and C. W. J. Beenakker, Phys. Rev. A **93**, 022329 (2016).

[20] M. Guo, S. Xia, N. Wang, D. Song, Z. Chen, and J. Yang, Opt. Lett. **45**, 6466 (2020).

[21] B. Xing, W. T. Chiu, D. Poletti, R. T. Scalettar, and G. Batrouni, Phys. Rev. Lett. **126**, 017601 (2021).

[22] A. L. S. Zameit, Photonics Res. **9**, A1 (2021).

[23] M. Wang, C. Doyle, B. Bell, M. J. Collins, E. Magi, and B. J. Eggleton, Nanophotonics **8**, 1327 (2019).

[24] Mordechai Segev, B. Crosignani, A. Yariv, and B. Fischer, Phys. Rev. Lett **68**, 923 (1992).

[25] H. S. Eisenberg, Y. Silberberg, R. Morandotti, A. R. Boyd, and J. S. Aitchison, Phys. Rev. Lett **81**, 3383 (1998).

[26] J. W. Fleischer, M. Segev, N. K. Efremidis, and D. N. Christodoulides, Nature (London) **422**, 147 (2003).

[27] M. J. Ablowitz, C. W. Curtis, and Y. Zhu, Phys. Rev. A **88**, 013850 (2013).

[28] M. J. Ablowitz and Y. Ma, Opt. Lett. **40**, 4635 (2015).

[29] A. Nunnenkamp, J. Koch, and S. M. Girvin, New J. Phys. **13**, 095008 (2011).

[30] S. Dutta and E. J. Mueller, Phys. Rev. A **97**, 033825 (2018).

[31] P. Roushan, C. Neill, A. Megrant, Y. Chen, R. Babbush, R. Barends, B. Campbell, Z. Chen, B. Chiaro, A. Dunsworth, A. Fowler, E. Je, J. Kelly, E. Lucero, J. Mutus, P. J. J. O. Malley, M. Neeley, C. Quintana, D. Sank, A. Vainsencher, J. Wenner, T. White, E. Kapit, and H. Neven, Nat. Phys. **13**, 146 (2017).

[32] V. Peano, M. Houde, C. Brendel, F. Marquardt, and A. A. Clerk, Nat. Commun. **7**, 10799 (2016).

[33] R. Kruse, F. Katzschmann, A. Christ, A. Schreiber, S. Wilhelm, K. Laiho, A. Gábris, C. S. Hamilton, I. Jex, and C. Silberhorn, New J. Phys. **15**, 083046 (2013).

[34] Y. Yang, P. Xu, L. L. Lu, and S. N. Zhu, Phys. Rev. A **90**, 043842 (2014).

[35] J. G. Titchener, A. S. Solntsev, and A. A. Sukhorukov, Phys. Rev. A **92**, 033819 (2015).

[36] J. G. Titchener, A. S. Solntsev, and A. A. Sukhorukov, Phys. Rev. A **101**, 023809 (2020).

[37] A. S. Solntsev, T. Liu, A. Boes, T. G. Nguyen, C. W. Wu, F. Setzpfandt, A. Mitchell, D. N. Neshev, and A. A. Sukhorukov, Appl. Phys. Lett. **111**, 261108 (2017).

[38] Y. Yang, P. Xu, L.-L. Lu, and S.-N. Zhu, Commun. Theor. Phys. **65**, 219 (2016).

[39] A. S. Solntsev, A. A. Sukhorukov, D. N. Neshev, and Y. S. Kivshar, Phys. Rev. Lett. **108**, 023601 (2012).

[40] C. S. Hamilton, R. Kruse, L. Sansoni, C. Silberhorn, and I. Jex, Phys. Rev. Lett. **113**, 083602 (2014).

[41] D. Leykam, A. S. Solntsev, A. A. Sukhorukov, and A. S. Desyatnikov, Phys. Rev. A **92**, 033815 (2015).

[42] Y. F. Bai, P. Xu, L. L. Lu, M. L. Zhong, and S. N. Zhu, J. Opt. **18**, 055201 (2016).

[43] M. A. Gorlach and A. N. Poddubny, Phys. Rev. A **95**, 053866 (2017).

[44] A. Blanco-redondo, B. Bell, D. Oren, B. J. Eggleton, and M. Segev, Science **362**, 568 (2018).

[45] Y. Wang, X. L. Pang, Y. H. Lu, J. Gao, Y. Chang, L. F. Qiao, Z. Q. Jiao, H. Tang, and X. M. Jin, Optica **6**, 955 (2019).

[46] S. Shen, *Topological Insulators* (Springer, Singapore, 2017).

[47] Q. Cheng, Y. Pan, Q. Wang, T. Li, and S. Zhu, Laser Photon. Rev. **9**, 392 (2015).

[48] T. Fukui, Y. Hatsugai, and H. Suzuki, J. Phys. Soc. Jpn. **74**, 1674 (2005).

[49] Y. Bromberg, Y. Lahini, R. Morandotti, and Y. Silberberg, Phys. Rev. Lett. **102**, 253904 (2009).

[50] A. S. Solntsev, F. Setzpfandt, A. S. Clark, C. W. Wu, M. J. Collins, C. Xiong, A. Schreiber, F. Katzschmann, F. Eilenberger, R. Schiek, W. Sohler, A. Mitchell, C. Silberhorn, B. J. Eggleton, T. Pertsch, A. A. Sukhorukov, D. N. Neshev, and Y. S. Kivshar, Phys. Rev. X **4**, 031007 (2014).

[51] H. Jin, F. M. Liu, P. Xu, J. L. Xia, M. L. Zhong, Y. Yuan, J. W. Zhou, Y. X. Gong, W. Wang, and S. N. Zhu, Phys. Rev. Lett **113**, 103601 (2014).

[52] X. W. Luo, Q. Y. Zhang, P. Xu, R. Zhang, H. Y. Liu, C. W. Sun, Y. X. Gong, Z. D. Xie, and S. N. Zhu, Phys. Rev. A **99**, 063833 (2019).

[53] J. Eisert, M. Cramer, and M. B. Plenio, Rev. Mod. Phys. **82**, 277 (2010).

[54] J. Tambasco, G. Corrielli, R. J. Chapman, A. Crespi, O. Zilberberg, R. Osellame, and A. Peruzzo, Sci. Adv. **4**, 3187 (2018).

[55] V. Peano, M. Houde, F. Marquardt, and A. A. Clerk, Phys. Rev. X **6**, 041026 (2016).

[56] Y. Wang, Y. H. Lu, F. Mei, J. Gao, Z. M. Li, H. Tang, S. L. Zhu, S. Jia, and X. M. Jin, Phys. Rev. Lett. **122**, 193903 (2019).